Linearity and Nonlinearity in Hollow-Core Antiresonant Fiber Sensors in the Terahertz Regime

Jakeya Sultana, Md. Saiful Islam, Md. Selim Habib, Mayank Kaushik, Alex Dinovitser, Brian W.-H. Ng, and Derek Abbott

In nonlinear optics, a major challenge is to maximize the interaction between the light from laser sources and low-density media such as gases. An ultrafast laser beam can be focused to form a highly intense spot over a small concentrated area. The ultrafast laser beam has a short pulse width of less than one picosecond and high peak power in the beam profile (Fig. 1). The beam profile of the laser source describes the energy density and distribution of light, and the beam profile of a laser source is usually affected during the propagation and collimation of the beam. An efficient nonlinear optical sensor also requires high peak power at low energy (low average power) over short duration of laser pulse, a high beam profile and long interaction length. These requirements of a nonlinear optical sensor with low attenuation constant can be achieved in hollow-core photonic crystal fiber (HC-PCF). Gas-filled HC-PCF exhibits optical nonlinearity for an ultrashort temporal and spectral broadening of NIR pulses [1], [2]. The nonlinearity in HC-PCF can be achieved by tuning the gas pressure.

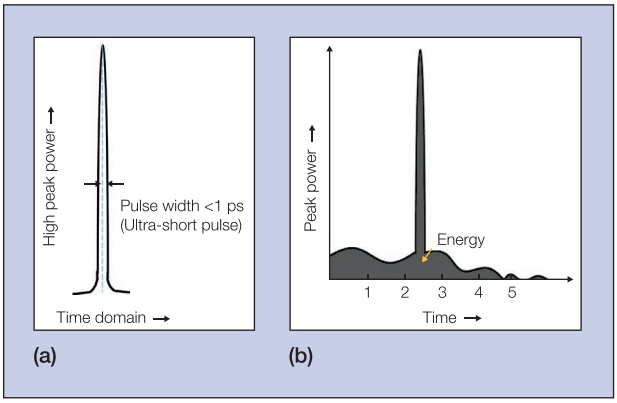

Fig. 1. (a) An ultrashort pulse with high peak power over a very short duration of pulse width and low average power. The laser has a short pulse width of less than one picosecond and high energy in the beam profile. (b) The graphical representation for power and energy throughout laser pulses. Peak power can be defined as the ratio of single pulse energy and the pulse width. Pulse energy corresponds to the area under the pulse shape. The average power denoted as the multiplication of single pulse energy and repetition time. The short duration of the laser pulse prevents the sensor damage by lowering the average power.

Gas-filled HC-PCF nonlinear media are low-cost, replenishable, reconfigurable and exhibit sharp spectral lines [3]. Linear and nonlinear responses are also found in other types of optical fibers.

For example, recently a single-mode fiber (SMF)/multimode fiber (MMF)/SM quasi two-mode fiber was reported for temperature measurements [4]. Similarly, an optical sensor built as a cascade of SMF/HCF/HC-PCF filled with ethanol can sense the refractive index and temperature of the liquid ethanol simultaneously [5], or a cascade of SMF/HCF/No core fiber (NCF)/PCF filled with liquid crystal/NCF/SMF measures the electric field sensitivity with the strain (tension) from the reflection and transmission spectrum [6]. For the reported sensors [4]–[6], a nearly linear relation between the peak wavelength and the temperature or refractive index or electric field intensity was observed. A magnetic field sensor based on a surface plasmon resonance (SPR) has also been reported to detect magnetic fluids [7]. Using silver as a plasmonic material to coat the fiber, the surface plasmon effect on the fiber surface was observed. Due to the plasmonic effect, this sensor shows nonlinear sensing characteristics.

Graphene has also been used to enhance the sensing performance. Recent work on metal-graphene coated fiber-based SPR sensors was theoretically analyzed for liquid analyte detection [8]. The reported sensor shows an enhancement in sensitivity when using graphene. Because of the nonlinearity of graphene and metal, this sensor also exhibits nonlinear sensing performance. A range of other nonlinear effects such as supercontinuum generation [9], high-harmonic generation [10], etc. have also been demonstrated in both resonant and antiresonant modes [11]–[13]. However, research-based on such nonlinearities in the terahertz regime has not been previously addressed.

An open research problem is the lack of high power terahertz laser sources that can create linear and nonlinear pulses simultaneously for nonlinear applications such as terahertz supercontinuum generation, terahertz high harmonic generation, etc. In this article, we model and simulate a simple hollow-core antiresonant terahertz waveguide, show the

1094-6969/21/$25.00©2021IEEE

linear properties and explore the mechanism of achieving nonlinearity with the established technology. First, the linear properties of HC antiresonant fiber (ARF) are discussed, and then the nonlinear properties of the same structure are demonstrated, considering a gas-filled core in the terahertz regime.

Anti-resonant Hollow Core Waveguide

The HC-ARF holds numerous attractive properties including low transmission loss in a broad bandwidth, high core power fraction and low interaction of core power with the surrounding polymer structure, and low dispersion [14]. The cross-section of the HC-ARF shown in Fig. 2a consists of a single layer of seven anti-resonant cladding tubes (with diameter D and Zeonex web thickness t) surrounding a central air defect. For guidance in the terahertz regime, the typical core diameter here ranges up to 3 mm with the tube web thickness of 0.09 mm. To explain the optical guiding mechanism of the proposed HC-ARF, the most commonly used anti-resonant reflecting optical waveguide (ARROW) model and the coupled-mode model are considered. In ARF, the thin membranes (web) in the cladding surround a central hollow core region and provide high reflection to confine and guide light in the hollow-core. The transmission and the reflection coefficient of these membranes depend on the polymer web thickness and refractive index of the material and the frequency of light in the fiber. The linearly polarized LP_{01} mode is considered as a dominant and fundamental mode as there is no power degradation. The LP_{01} mode shown in Fig. 2b is localized at the central hollow core for the straight fiber. Fig. 2c shows the schematic of LP_{01} mode using the red curve in the core. The thin membrane of the cladding tube reflects most of the light and confines it in the central core. Here, the dashed arrow inside the red curve exhibits the electric field intensity (E).

FEM Modelling

We develop a 2D model using the finite element method (FEM) based software Comsol Multiphysics v5.4. Here the Wave Optics module is used to investigate the optical properties such as loss, dispersion and mode field patterns. The sensitivity of the proposed HC-ARF changes with the refractive index variation. Proper choice of mesh dimensions increases the computational accuracy, and to that end, we use the *extremely fine* element size in a physical controlled mesh sequence. A perfectly matched layer (PML) that is also known as absorbing boundary condition is used at the outside the fiber structure to accurately predict the leakage loss.

Linear Properties of HC-ARF

The modified capillary model shown in Fig. 2a is used to calculate the effective refractive index for the linearly polarized LP_{01}-like fundamental mode that is shown in Fig. 3a. Fig. 3a indicates that the effective refractive index (η_{eff}) of the LP_{01}-like fundamental mode increases linearly with the frequency. The mode field profile of the LP_{01}-like fundamental mode shown in Fig. 3c indicates the strong field confinement inside the core, which is desirable for obtaining low transmission loss at 1 THz frequency. Also, the LP_{01}-like fundamental mode indicates the effect of cladding resonance at 1.6 THz, as power couples between the core mode and the surrounding thin Zeonex webs.

The degree of transmission loss is fully dependent on the core size and thickness of the cladding web. The obtained loss in the fundamental mode is illustrated in Fig. 3b. The physics of the resonance peaks (high leakage loss) obtained in Fig. 3b can be recognized as the radial resonances of light with the concentric Zeonex structure. There is the coupling of power between the core modes and the Zeonex webs. The fraction of power (FOP) in the polymer web, shown in Fig. 3b, indicates a significant increase of FOP at cladding resonances, ~1.6 THz, 2.5 THz, etc. where light from the core strongly couples with the polymer web. It is important to locate the central frequency far away from resonance by tuning the web thickness to avoid damage to the fiber; this keeps the damage threshold high. There is very low power coupling (0.01%) to the surrounding polymer web. The FOP in the polymer web is used to calculate the effective material loss (EML). The EML is then added to leakage loss and this yields the total propagation loss. Apart from the resonance peaks, the HC-ARF provides broadband guidance (0.62–1.60 THz) at a low loss of ~1 dB/m around 1 THz.

In Fig. 4, we illustrate the fraction of power passing through the hollow core, the relative sensitivity and the dispersion profile of the HC-ARF. Fig. 4a shows the amount of light and analyte interaction of the fundamental LP_{01} mode within the core for different analytes as a function

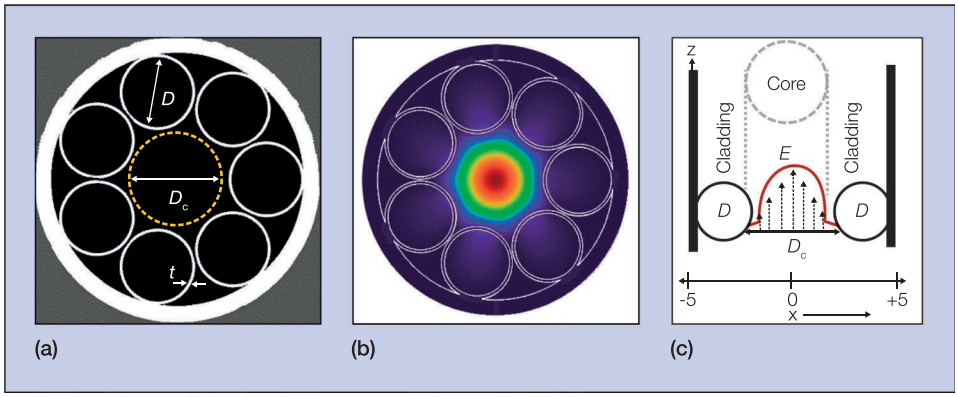

Fig. 2. (a) Cross-section of a proposed HC-ARF, showing seven non-touching air holes in the cladding. (b) Modal field intensity of LP_{01}-like fundamental mode at 1 THz. (c) Schematic representation of LP_{01}-like fundamental mode (red curve) and corresponding electric field pattern (dashed arrow).

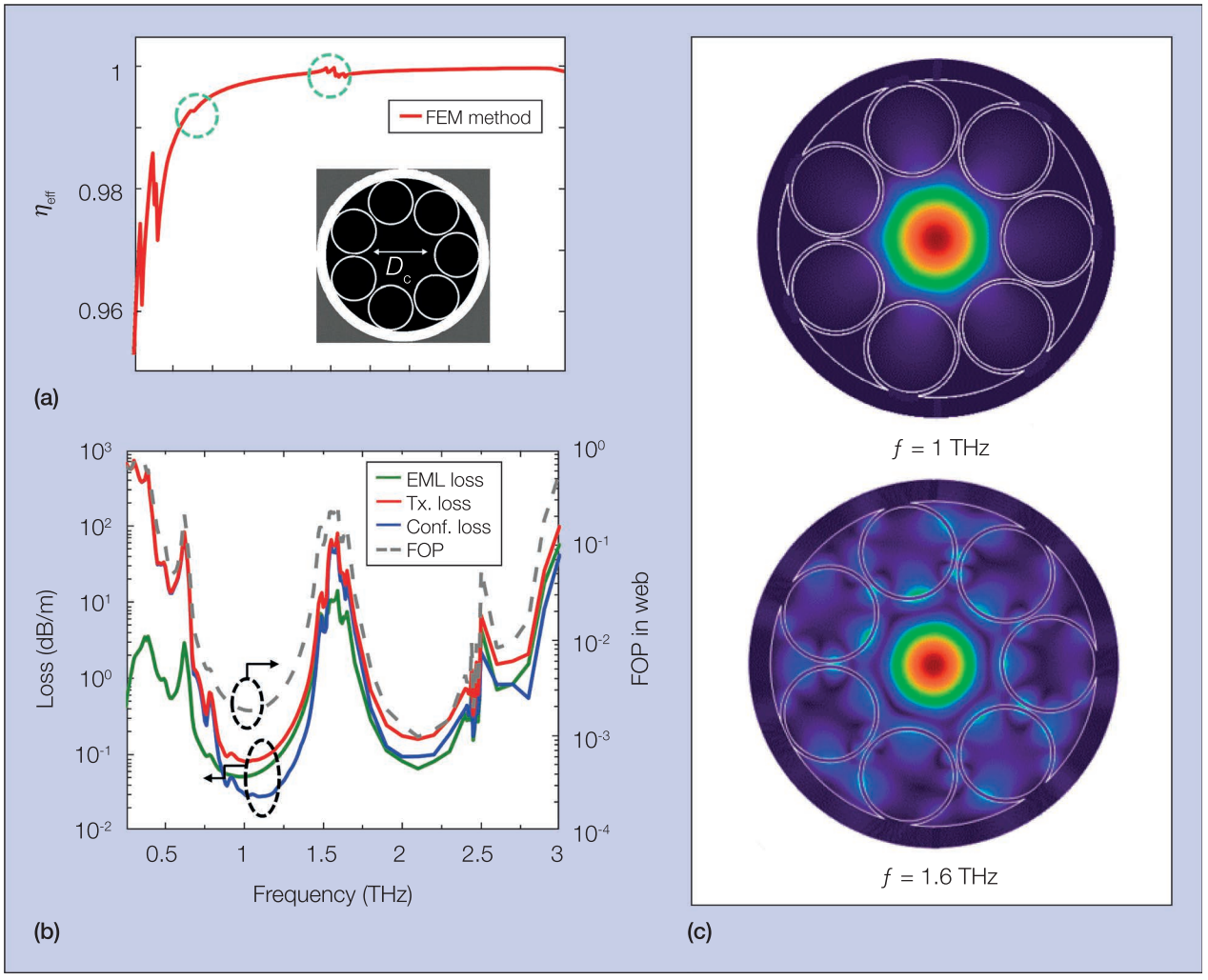

Fig. 3. Calculations from simulations performed using an FEM approach. (a) Effective refractive index (η_{eff}) of LP_{01}-like fundamental mode, (b) effective material loss (EML), confinement loss, transmission loss (left) and fraction of power (FOP) in polymer web (right) of an evacuated HC-ARPCF with a 3 mm core diameter, and 0.09 mm polymer web; (c) Mode field intensity plots of two computed modes at 1 THz (on antiresonance) and 1.6 THz (on-resonance).

of frequency. The numerical simulation reveals that more than 99% of power concentrates within the hollow region at around 1 THz. The modal power distributions employing different refractive indices in the core explain the spectral behavior of the filled analytes. Fig. 4b represents the relative sensitivity of the HC-ARF by varying the analyte refractive index. In our analysis shown in Fig 4c, the theoretical maximum refractive index sensitivity for the proposed sensor is 3335 GHz/RIU (refractive-index-unit) [15].

The group velocity dispersion (GVD) and the power flow through the core are shown in Fig. 4d. We can see that over 99.99% of the light can be guided through the core region. The cladding resonance disrupts the transmission and therefore has very little impact on the GVD. The low dispersion slope implies that, even though the material nonlinearity for Zeonex is relatively weak, the nonlinear contribution to the phase-matching is significant. It displays almost flat and zero GVD for the LP_{01}-like fundamental mode. With the advantage of having a much lower transmission loss, an HC-ARF fiber is linear with a zero dispersion for the entire frequency range which is verified through FEM simulation shown in Fig. 4d (green curve). The shallow and flat GVD slope changes rapidly at resonance frequencies where the refractive index of the core mode and cladding mode matches and causes strong coupling between them.

Although a HC-ARF exhibits zero dispersion, it has a close to zero nonlinear coefficient because of its low FOPS (<< 0.01%) in the material; however, there are ways to create nonlinearity in the terahertz regime. HC-ARFs provide anomalous dispersion which is suitable for chirped pulse compression by self-phase modulation (SPM). This facilitates linear or near-linear dispersive compression, analogous to what can be acquired through bulk diffraction gratings, in an all-fiber system at pulse energies where standard fibers would be strongly nonlinear. The GVD plays the central role in controlling the nonlinear dynamics, the dispersion properties of which can be extensively engineered by varying the gas species or the gas pressure—this has become the dominant approach for exploring the nonlinear effect in gas-filled HC-ARF.

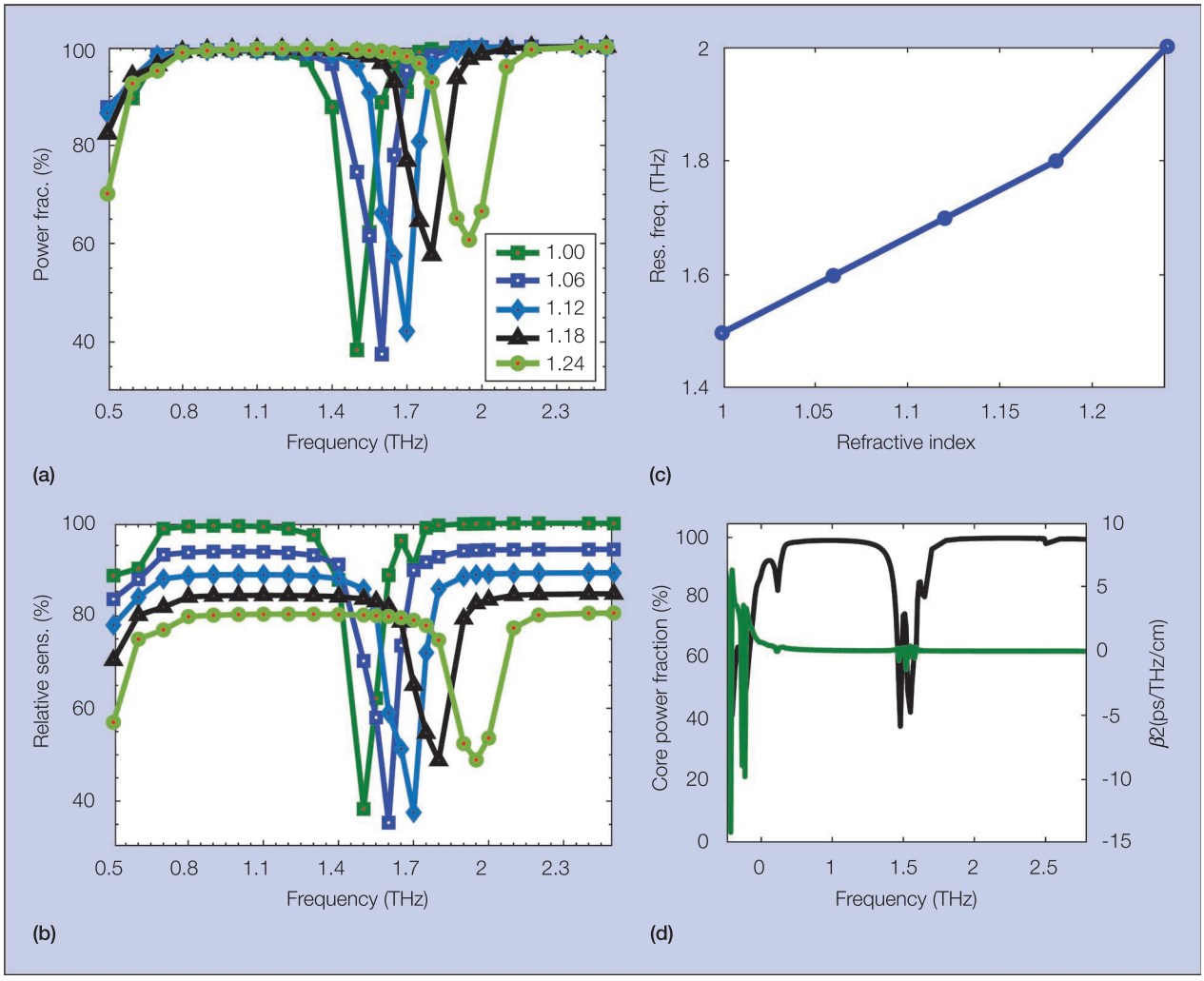

Fig. 4. (a) Core power fraction for different analytes of the proposed gas sensor [15], used with permission ©IEEE. (b) Relative sensitivity of the proposed gas sensor [15], used with permission ©IEEE. (c) Change of resonance frequency with the change of refractive index. (d) Calculated group velocity dispersion (GVD) of an evacuated HC-ARPCF with a 3 mm core diameter, and 0.09 mm polymer web (green curve).

Comparison between Linear and Nonlinear Properties of HC-PCF

In this section, we outline the linear and nonlinear properties of different HC-PCF and determine the best candidate for nonlinear fiber sensing. Based on guiding mechanisms, HC-PCF comes in two main varieties. The first is a photonic bandgap (PBG) fiber shown in Fig. 5a that exhibits low loss, confines light strongly, and the GVD has a steep slope that makes it suitable for spectral filtering.

The second type of HC-PCF has a kagomé lattice cladding shown in Fig. 5b that can exhibit ultra-broadband guidance of light with extremely low loss and displays weak anomalous GVD over the entire transmission window employing a low dispersion slope. The kagomé-lattice fiber can also exclude the anticrossing with a strong cladding resonance. These cladding resonances are quite narrow and disrupt the transmission window, and therefore, they have very little impact on dispersion properties [2].

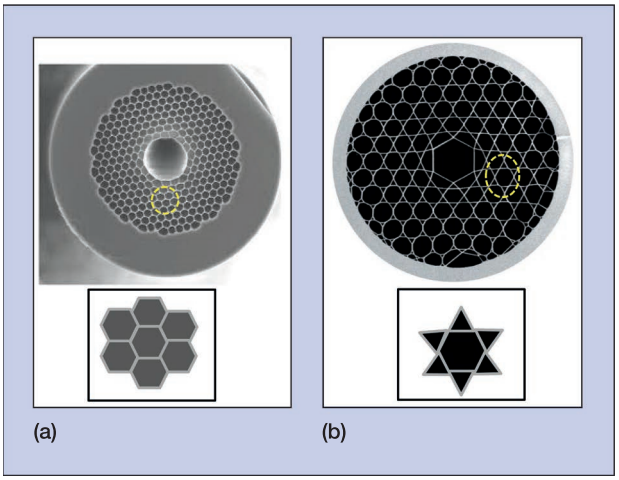

Fig. 5. Cross-section of HC-PCF in (a) photonic bandgap style and (b) kagomé style [1], with their corresponding enlarged cladding patterns. Images used with permission from [1], © The Optical Society.

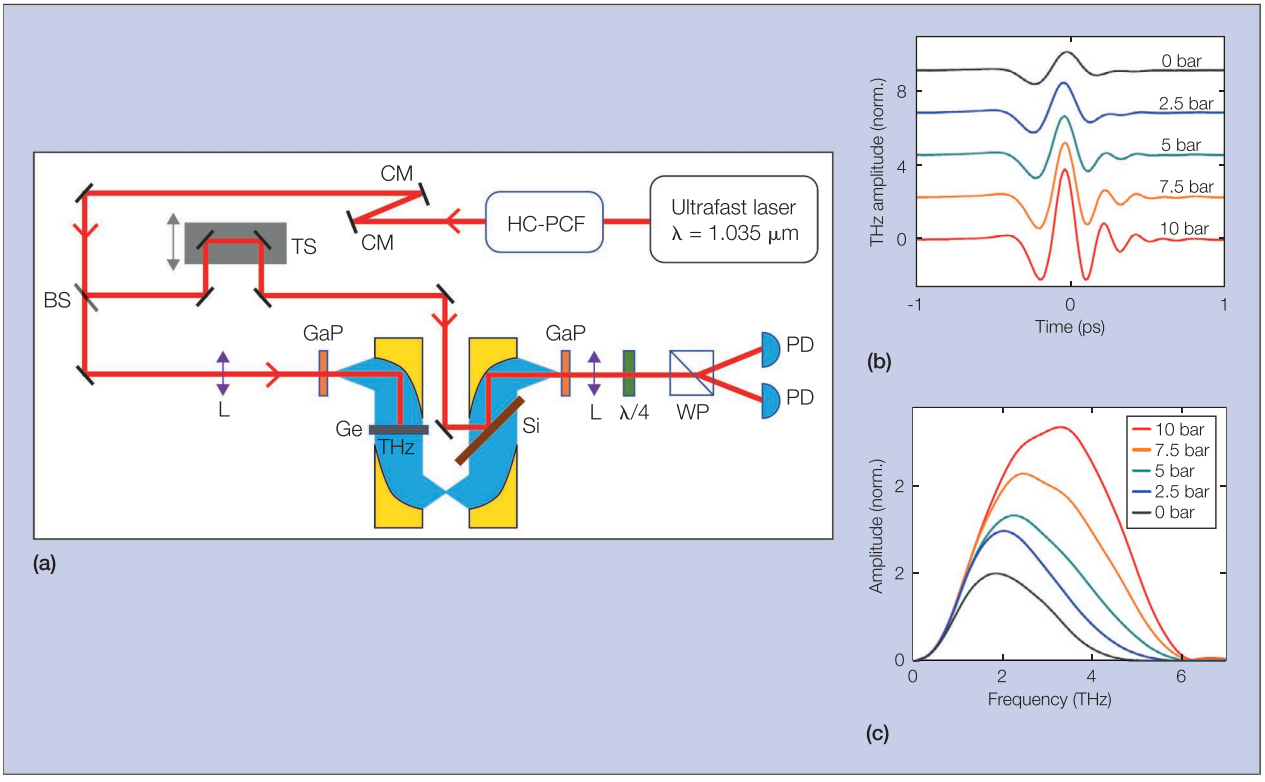

Fig. 6. (a) Schematic of the experimental setup to achieve broadband terahertz generation and detection. CM: chirped mirror; BS: beam splitter; TS: translational stage; L: lens, GaP: <110>-oriented 220 μm -thick gallium phosphide crystal; Ge: germanium wafer; Si: silicon wafer; λ/4: quarter-wave plate; WP: Wollaston prism; PD: photodetector. (b) Temporal amplitude recorded with terahertz lock-in amplifier prepared in the HC-PCF at different Ar pressures. (c) Corresponding THz spectral amplitude [16], used with permission under a Creative Commons Attribution (CC BY) license.

Note that, the dispersion properties of kagomé cladded PCF in Fig. 5b and the capillary cladded ARF in Fig. 2a are similar; however, the transmission losses of these two are different. At the same core diameter, the kagomé cladded fiber exhibits significantly lower loss than capillary cladded fiber. However, considering fabrication feasibility, capillary cladded fiber is simpler than the kagomé fiber. Therefore, it is more practical to use capillary cladded fiber for any nonlinear applications.

Ways to Create Nonlinearities in HC-ARF

In a hollow core terahertz fiber, the possible nonlinearities can be obtained following the experimental setup proposed by Cui *et.al* [16]. In a gas-filled environment, the HC-ARF can be used to broaden the terahertz spectrum. The proposed terahertz system setup can be used with a stable MHz laser that can deliver pulses of sub-microjoule energy and duration of a few hundred femtoseconds.

A Yb:KGW ultrafast laser amplifier propagates near-infrared (NIR) pulses as an optical source shown in Fig. 6a. The ARF in a gas-filled environment can be used to compress the NIR pulses for efficient broadband terahertz spectrum by varying the gas pressure. Here, the linear and nonlinear properties of the HC-ARF can be controlled by controlling the gas pressure that also permits the optimization of pulse spectral broadening.

To compensate for the positive chirp induced from self-phase modulation (SPM), a pair of identical chirped mirrors can be placed after the HC-ARF. A beam splitter divides the NIR pulses into linear pump pulse and probe pulse where two nonlinear gallium phosphide (GaP) crystals are used for terahertz generation and detection, respectively, based on optical rectification. The emitted terahertz pulses from GaP are collected and focused on the identical detection crystal (GaP) using parabolic mirrors. The terahertz pulse in detection crystal and the pump pulse together allow coherent detection. When the terahertz electric field penetrates along the one axis of the nonlinear detection crystal, the variations in crystal refractive index create birefringence in the terahertz electric field, which is assumed linearly polarized at the beginning. A quarter-wave plate has two perpendicular axes and decomposes the electric field as E_x and E_y. When the quarter-wave plate is not oriented at 45°, to the elliptically polarized electric field, it adds $\varpi/2$ dephasing for both components. A suitably oriented Wollaston prism (WS: two triangular prisms interfaced together) provides the intensities for both orthogonal components. The intensity mismatch is measured using two photodetectors. This detection procedure, known as electro-optic sampling, has been applied for coherent pulse detection to accurately recover the phase difference and amplitude of two orthogonal components. The nonlinear crystal modifies the polarization state of the terahertz electric field, and by resolving the change in polarization, it is possible to directly map the terahertz electric field. As the gas pressure increases from 0 to 10 bar, the peak terahertz amplitude increases due

to temporal compression of the NIR pulses, leading to higher peak powers and, consequently, to more efficient nonlinear frequency down-conversion illustrated in Fig 6b. The corresponding terahertz spectral amplitudes are shown in Fig. 6c. The development of an efficient terahertz system with a broadband spectral window can allow the access of molecular resonance for sensing applications.

Conclusion

In this article, a novel approach for preparing ultrashort pulses from gas-filled antiresonant fiber has been presented to achieve efficient broadband terahertz generation and detection. The linear properties of an evacuated waveguide become nonlinear by tuning the gas pressure, creating a broadband terahertz spectrum due to SPM. The approach is extremely interesting due to the low cost of the technology and the simplicity of the waveguide architecture. The development of efficient terahertz systems with broadband spectral window can allow the access of molecular resonances for ultrasensitive sensing applications.

References

[1] J. C. Travers, W. Chang, J. Nold, N. Y. Joly, and P. S. J. Russell, "Ultrafast nonlinear optics in gas-filled hollow-core photonic crystal fibers (invited)," *J. Opt. Soc. Am. B*, vol. 28, A11-A26, 2011.

[2] P. S. J. Russell, P. Hölzer, W. Chang, A. Abdolvand, and J. C. Travers, "Hollow-core photonic crystal fibres for gas-based nonlinear optics," *Nat. Photon.*, vol. 8, pp. 278-286, 2014.

[3] M. C. Downer, "A new low for nonlinear optics," *Science*, vol. 298, pp. 373-375, 2002.

[4] M. Olivero, A. Vallan, R. Orta and G. Perrone, "Single-mode–multimode–single-mode optical fiber sensing structure with quasi-two-mode fibers," *IEEE Trans. Instrum. Meas.*, vol. 67, no. 5, pp. 1223-1229, May 2018.

[5] Y. Zhao, X.-G. Li, L. Cai, and Y.-N. Zhang, "Measurement of RI and temperature using composite interferometer with hollow-core fiber and photonic crystal fiber," *IEEE Trans. Instrum. Meas.*, vol. 65, no. 11, pp. 2631-2636, 2016.

[6] X.-G. Li, Y.-N. Zhang, X. Zhou, and L. Cai, "Simultaneous measurement of electric field and strain with a tandem-interferometric device," *IEEE Trans. Instrum. Meas.*, vol. 67, no. 4, pp. 965-970, 2018.

[7] X. Zhou, X. Li, S. Li, G. An and T. Cheng, "Magnetic field sensing based on SPR optical fiber sensor interacting with magnetic fluid," *IEEE Trans. Instrum. Meas.*, vol. 68, no. 1, pp. 234-239, Jan. 2019.

[8] A. A. de Melo, T. B. da Silva, M. F. da Silva Santiago, C. da Silva Moreira and R. M. S. Cruz, "Theoretical analysis of sensitivity enhancement by graphene usage in optical fiber surface plasmon resonance sensors," *IEEE Trans. Instrum. Meas.*, vol. 68, no. 5, pp. 1554-1560, May 2019.

[9] P. B. Corkum, C. Rolland, C., and T. Srinivasan-Rao, "Supercontinuum generation in gases," *Phys. Rev. Lett.*, vol. 57, pp. 2268-2271, 1986.

[10] T. Popmintchev, M.-C. Chen, P. Arpin, M. M. Murnane & H. C. Kapteyn, "The attosecond nonlinear optics of bright coherent X-ray generation," *Nature Photon.*, vol. 4, pp. 822-832, 2010.

[11] L. Allen, and J. H. Eberly, *Optical Resonance and Two-Level Atoms*. New York, NY, USA: John Wiley and Sons, 1975.

[12] J. F. Reintjes, *Nonlinear Optical Parametric Processes in Liquid and Gases*. Cambridge, MA, USA: Academic Press, 1984.

[13] P. H. Y. Lee, D. E. Casperson, G. T. Schappert, and G. L. Olson, "X-ray generation from subpicosecond superintense laser atom–interaction," *J. Opt. Soc. Am. B*, vol. 7, pp. 272-275, 1990.

[14] V. Setti, L. Vincetti, and A. Argyros, "Flexible tube lattice fibers for terahertz applications," *Opt. Express*, vol. 21, pp. 3388-3399, 2013.

[15] J. Sultana, M. S. Islam, C. M. B. Cordeiro, M. S. Habib, M. Kaushik, A. Dinovitser, B. W.-H. Ng, H. Ebendorff-Heidepriem, and D. Abbott, "Hollow core inhibited coupled antiresonant terahertz fiber: a numerical and experimental study," *IEEE Trans. Terahertz Sci. Technol.*, 2020.

[16] W. Cui, A. W. Schiff-Kearn, E. Zhang, N. Couture, F. Tani, D. Novoa, P. S.J. Russell, and J-M. Ménard, "Broadband and tunable time-resolved THz system using argon-filled hollow-core photonic crystal fiber," *APL Photon.*, vol. 3, 111301, 2018.

Jakeya Sultana (jakeyaete09ruet@gmail.com) received the B.Sc. degree from Rajshahi University of Engineering and Technology and the M.Sc. degree from Islamic University of Technology, Bangladesh in 2014 and 2017, respectively. She is a Ph.D. degree candidate in the School of Electrical and Electronic Engineering of The University of Adelaide, Australia. Her research interests include anti-resonant fibers for terahertz application and super-continuum generation.

Md. Saiful Islam (M'18) is conducting Ph.D. research in the School of Electrical and Electronic Engineering at The University of Adelaide, Australia. His research interests include optical fiber communication, PCF based terahertz waveguides, terahertz sensors, surface plasmon resonance biosensors, topological insulators, metamaterials for sensing applications.

Md. Selim Habib (S'13–SM'19) is an Assistant Professor of Electrical and Computer Engineering at Florida Polytechnic University in Lakeland, Florida. He received the B.Sc. and M.Sc. degrees in electrical and electronic engineering from Rajshahi University of Engineering Technology, Rajshahi, Bangladesh in 2008 and 2012, respectively. He received the Ph.D. degree in photonics engineering from Technical University of Denmark, Copenhagen, Denmark, in 2017.

Mayank Kaushik as been a Research Scientist with the the Defense Science and Technology Organisation, Edinburgh, Australia since March 2012. He obtained a bachelor's degree in electronic and telecommunication engineering in 2005 from the NRI Institute of Information Science and Technology at Bhopal, India. In 2006, he received his Master's Degree in Electronic and Telecommunication Engineering (Adv.), from the University of Adelaide in December 2007. In 2013, he received his PhD from the University of Adelaide in Electrical and Electronic Engineering.

Alex Dinovitser (M'18) is a Postdoctoral Fellow at The University of Adelaide, Australia. He has worked within the

electronics manufacturing industry, designing computer interface and signal acquisition systems. In 2008, he built the first spectroscopic lidar in Australia for the differential absorption detection of atmospheric trace gasses.

Brian Wai-Him Ng is a Senior Lecturer at the School of Electrical and Electronic Engineering, University of Adelaide. His research interests include radar signal processing, wavelets and terahertz (T-ray) signal processing. He is currently an active member within the South Australian Chapter of the IEEE.

Derek Abbott (M'85-SM'99-F'05) has been with The University of Adelaide, Australia since 1987 and is currently a full Professor with the School of Electrical and Electronic Engineering. He received the B.Sc. degree in physics from Loughborough University, Leicestershire, UK in 1982 and the Ph.D. degree in electrical and electronic engineering from The University of Adelaide, Australia in 1995. His research interests include multidisciplinary physics and electronic engineering applied to complex systems, networks, game theory, energy policy, stochastics, and biophotonics.

augustcalendar

For more information on these and other meetings, please go to the I&M Society Web site at www.ieee-ims.org.

SAS 2021/August 2-4, 2021 (virtual event)
IEEE Sensors Applications Symposium
Sundsvall, Sweden
https://2021.sensorapps.org/

IST 2021/August 24-26, 2021 (virtual event)
IEEE International Conference on Imaging Systems and Techniques
Kaohsiung, Taiwan
https://ist2021.ieee-ims.org/

AUTOTESTCON 2021/(canceled)
AUTOTESTCON
Oxon Hill (National Harbor), MD
https://autotestcon.com/

AMPS 2021/September 29-October 1, 2021 (virtual event)
IEEE International Workshop on Applied Measurements for Power Systems
Cagliari, Italy
https://ist2021.ieee-ims.org

ISPCS 2021/ October 26-28, 2021 (virtual event)
IEEE International Symposium on Precision Clock Synchronization for Measurement, Control, and Communication
https://2021.ispcs.org/

ROSE 2021/October 28-29, 2021 (virtual event)
IEEE International Symposium on RObotic and Sensors Environments
New York, NY, USA
https://rose2021.ieee-ims.org

ICCVE 2022/February 21-23, 2022 (hybrid event)
IEEE International Conference on Connected Vehicles and Expo
Lakeland, Florida, USA
https://iccve2022.org/

AUTOTESTCON 2022/August 28-31, 2022
AUTOTESTCON
Oxon Hill (National Harbor), Maryland, USA
https://2021.autotestcon.com/